J. Cent. South Univ. (2024) 31: 3807−3818
DOI: https://doi.org/10.1007/s11771-024-5799-9

Springer

Creep properties of bimetal Al/SiC/Cu composites fabricated via accumulative roll bonding process

Basem Ali[1], Jasim Dheyaa J.[2], Bansal Pooja[3, 4], Qasim Maytham T.[5], Brisset BJ.[6]*

1. Faculty of Engineering, Warith Al-Anbiyaa University, Karbala 56001, Iraq;
2. Department of Petroleum Engineering, Al-Amarah University College, Maysan, Iraq;
3. Department of Biotechnology and Genetics, Jain (Deemed-to-be) University, Bengaluru, Karnataka-560069, India;
4. Department of Allied Healthcare and Sciences, Vivekananda Global University, Jaipur, Rajasthan-303012, India;
5. College of Health and Medical Technology, Al-Ayen University, Thi-Qar, 64001, Iraq;
6. Institut des Matériaux Jean Rouxel (IMN), UMR 6502, Polytech'Nantes, Nantes Cedex, France

Abstract: In the present study, microstructural evolution, mechanical and creep properties of Al/SiC/Cu composite strips fabricated via accumulative roll bonding (ARB) process were studied. The obtained results showed the formation of an atomic diffusion layer with thickness of about 17 μm at the interface during the ARB under three creep loading conditions namely 30 MPa at 225 °C, 35 MPa at 225 °C, and 35 MPa at 275 °C. An generated intermetallic compound resulted in a 40% increase of interface thickness near Al. The stress level decreased by 13% at constant temperature with no significant effect on the interface thickness, and the creep failure time declined by 44%. It was observed that at constant temperatures, the second slope of the creep curve reached to 39% with increasing stress level, then, it dropped to 2% with a little temperature rising. After creep test under 35 MPa at 275 °C, the sample displays the presence of 60% Al and 40% Cu, containing brittle Al_2Cu intermetallic compound at the interface. Applied temperature and stress had effect on the creep properties, specially increasing the slope of creep curves with higher stresses.

Key words: creep property; intermetallic compounds; accumulative roll bonding; microstructure; bimetal

Cite this article as: Basem Ali, Jasim Dheyaa J., Bansal Pooja, Qasim Maytham T., Brisset BJ.. Creep properties of bimetal Al/SiC/Cu composites fabricated via accumulative roll bonding process [J]. Journal of Central South University, 2024, 31(10): 3807−3818. DOI: https://doi.org/10.1007/s11771-024-5799-9.

1 Introduction

Todays, it is so difficult for traditional materials to get necessary application in enhancing industries such as aerospace, automotive, and electronics. Consequently, there is a rising demand for laminated composites because they have several distinct properties together [1−7].

During last decades, application of lightweight structures has improved to reduce the fuel consumption with the rise of carbon dioxide in the atmosphere and the importance of protecting the environment [8−10].

Generally, alloys and metals have limited properties and it is impractical for them to include several needed properties together. As a new technique, manufacturing of bimetal or bi-alloy

Received date: 2023-11-21; **Accepted date:** 2024-05-02
Corresponding author: Brisset BJ., PhD, Assistant Professor; E-mail: bj.brisset@outlook.com; ORCID: https://orcid.org/0009-0006-3735-6926

composites is a new approach to achieve several-needed properties together. Bimetal Al/Cu composites have got interest due to their excellent properties such as high strength, easy recyclability, high specific stiffness, and high damping capacity. Moreover, they have good thermal and electrical conductivity of copper, and also low density and high corrosion resistance of aluminum [11−15].

As a novel approach to manufacture materials containing ultra-fine grain (UFG) structures, severe plastic deformation (SPD) is developed during the past few decades. Some of SPD processes include cyclic extrusion compression (CEC), multi axial forging (MAF), accumulative roll bonding (APB), accumulative press bonding (APB), and so on [16−23].

Accumulative roll bonding (ARB) is not only an SPD forming process, but also a bonding process (as a solid phase method of welding). So, metallic strips and foils bond together during cumulative rolling steps at high plastic strains. With the help of ARB, it is practicable to fabricate laminated composite strips and foils by cumulative rolling steps. Generally, the thickness reduction ratio for ARB is 50%. This process includes primary sample preparation (annealing and final sizing), surface brushing and cleaning in the acetone bath, and then, rolling with 50% reduction of thickness [24−30].

Over the past few years, many studies have been done on the mechanical properties of composites manufactured via SPD approaches. The creep property of these samples requires a thoroughly inquiry. In the matter of SPD, the study of creep properties has not gained considerable attention. So, USCINOWICZ et al [29, 31] proposed a relation between creep strain and applied stress for Al/Cu composites following an exponential pattern. Besides, the minimum creep rate is more important for TD samples than RD samples at a stress less than 120 MPa while the fronting is accurate for the maximum quantities (above 120 MPa). Furthermore, failure elongation in TD samples is not dependent of the stress levels while it increases with rising stress levels for RD samples. AVALLONE et al [30] revealed that the creep property of Cu-Nb composites fabricated via ARB is a function of bonding interface thickness which varies between 60 nm and 2 μm. They also realized that creep resistance enhances by generation of a UFG structure.

An investigation in the field of bonding properties of Al/Zn composites during the first and second creep stages demonstrated a nonlinear dependency between strain and stress rate [31]. TSAI et al [32] stated that St/Br composites experience faster creep at lower strain rates (below 0.001), which is caused by the help of grain size variations during the phase transformation. Also, these bimetal composites experience a little slower creep at high strain rates (above 0.001) and temperature higher than 810 °C due to the presence of more phase transformation in the type of muscular ferrite-to-austenite.

In this work, the Al/Cu bimetal composites reinforced with SiC_p fabricated through ARB have been manufactured, then, microstructural evolution, mechanical and creep properties were investigated via ARB parameters.

2 Experimental procedure

2.1 ARB process

Fully annealed pure copper and AA1050 are utilized in this study to manufacture bimetal Al/Cu composite strips. Annealing was carried out for a period of 2 h at 400 °C on all samples before the ARB process and then, samples were cooled in the ambient temperature. Surface preparation is a vital step before the ARB. During the roll bonding as a solid phased method of welding, metallic strips start to bond together. So, surfaces to be bonded must be free of any contaminations, as shown in Figure 1. These contaminations are absorbed ions, dust particles, oxide layers on surfaces, grease particles, etc. These contaminations are severe barriers against the extrusion of fresh virgin metals extruding normal to the rolling direction, as shown in Figure 2. Furthermore, the cleaner the surface to be bonded, the stronger the layers bonding. To this purpose, all surfaces that are going to be bonded were scratched with a rotary brush (a diameter of 90 mm, wire diameter of 0.3 mm with a rotary speed of 1500 r/min under a load of 15 N).

To clean the surfaces from grease, the next step is soaking brushed strips in the acetone bath for a period of 20 min. After that, SiC particles (SiC_p)

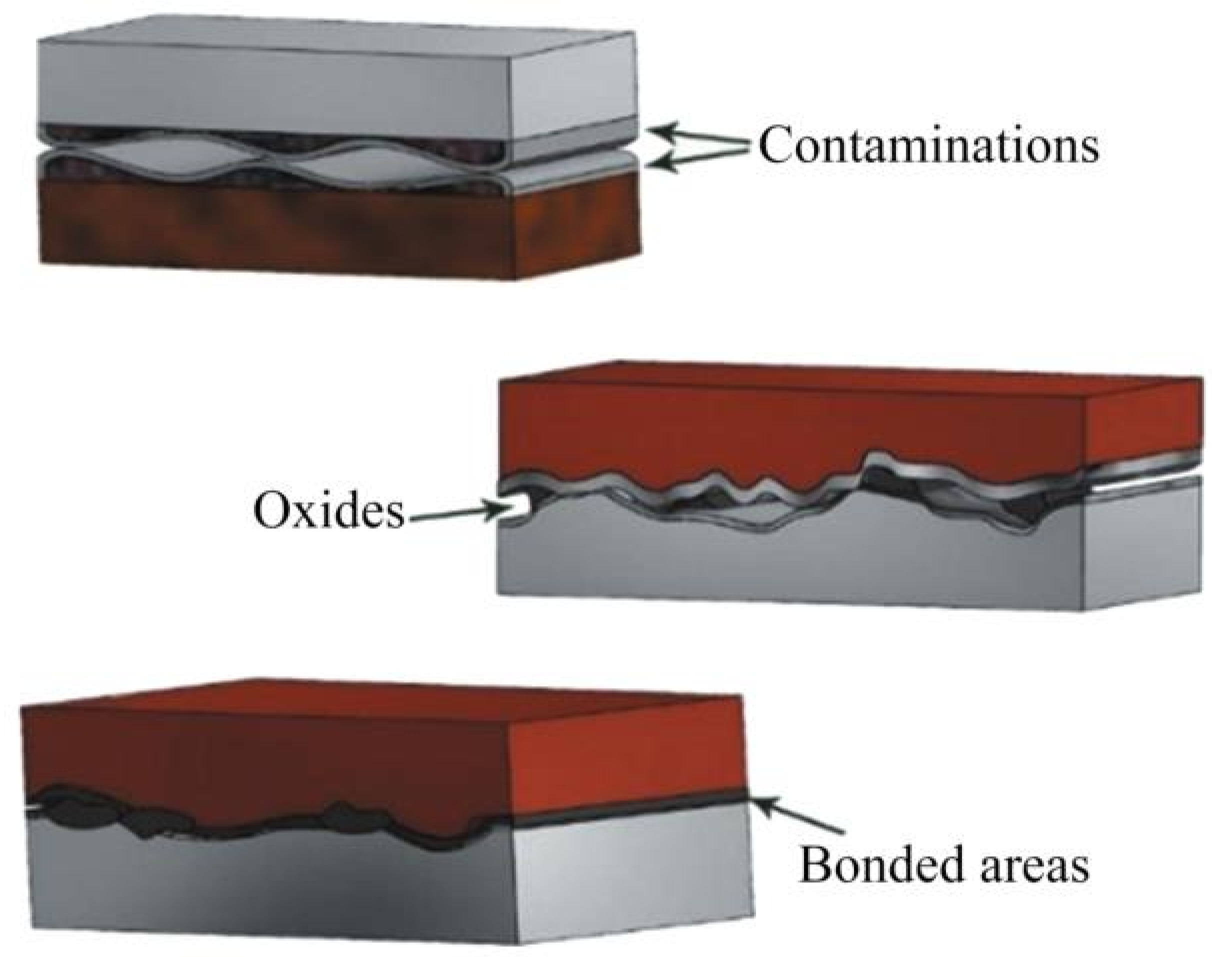

Figure 1 Bonding generation between two layers of Al and Cu under rolling pressure

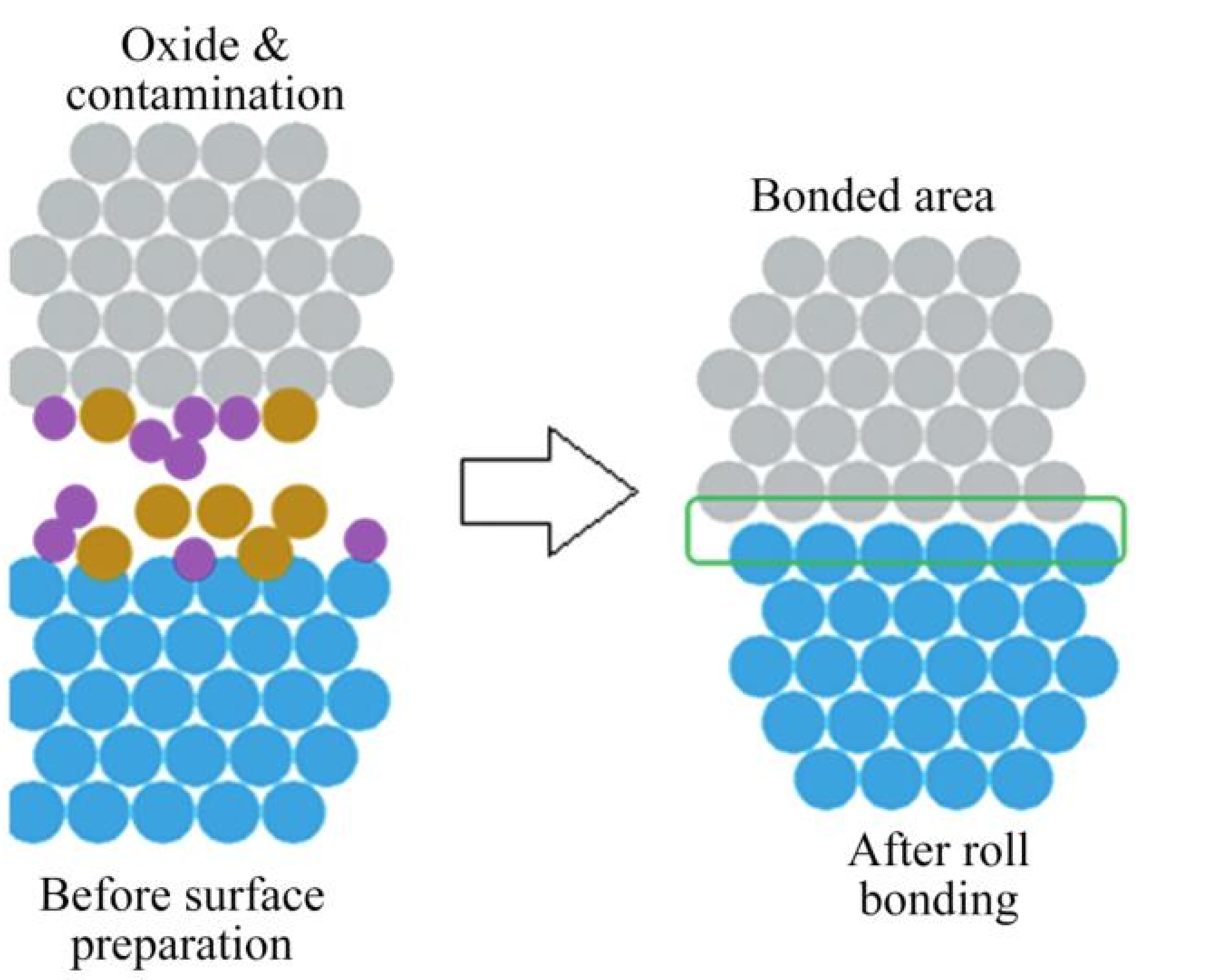

Figure 2 Existence of contaminations on surfaces to be bonded

with 2.5 wt%, 5 wt% and 7.5 wt% were added on surfaces while soaked in ethanol alcohol in an ultrasonic bath with a frequency of 60 kHz at 60 ℃ (in an oven) to get an unchanging dispersion of SiC particles. Finally, strip surfaces were covered consistently with SiC_p. Then, two strips were stacked together and their both ends were fastened by steel wires to avoid slipping. Stacked samples were rolled with a reduction ratio of 50%. Then, ARB was conducted up to 8 cycles with the mentioned sample preparations before each cycle, as shown in Figure 3. To set up the ARB, a rolling machine with a tonnage of 100 t was used. The plastic strain for each ARB step is:

$$\varepsilon_{eq}=\frac{2}{\sqrt{3}}N\left(\ln\frac{t_0}{t}\right)\frac{2}{\sqrt{3}}N\left(\ln\frac{1}{1-R}\right) \tag{2}$$

where N is number of ARB cycles; t is the final thickness; t_0 is initial thickness; ε_{eq} is equivalent plastic strain; R is the reduction in thickness ratio, respectively.

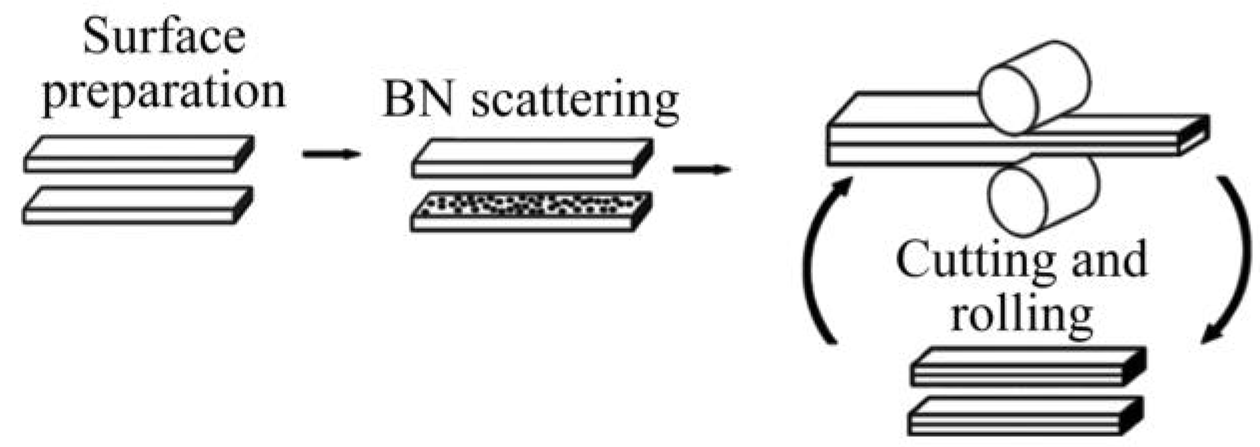

Figure 3 Schematic drawing of ARB process

To conduct tensile and Vickers hardness (HV) test, ASTM-E8M and ASTM-E384 standards were used, respectively. During the HV test, a force of 5 N for 15 s was applied as its testing conditions.

2.2 Creep test

In this stage, 11-133-E standard was referred for the creep test. The creep was done in the temperature range of 250−350 ℃ and stress range of 30−40 MPa on a SCT-35 creep testing machine. Figure 4 illustrates the drawing of the creep test setup used in this study.

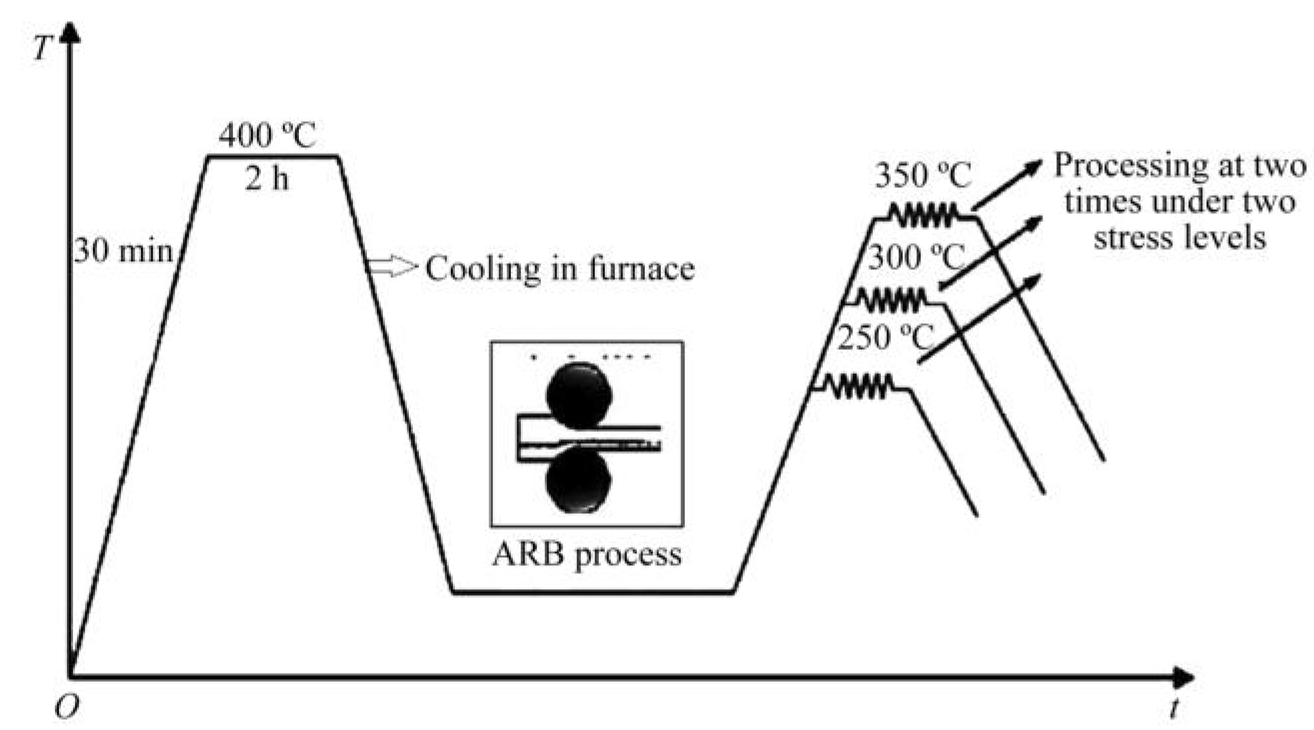

Figure 4 Process of ARB and creep test

Figure 5 shows the schematic illustration of the samples prepared for creep and tensile test, respectively. ASTM E139 standard was utilized to prepare the samples for the creep test. The test was performed with stress levels set under 30 and 35 MPa at 225 and 275 ℃. During the creep test, the applied stress and temperature were constant. After that, samples were positioned in the checking fixture in the furnace for 20 min to get a constant temperature during the creep test. During the fabrication process of samples and all tests, the ambient temperature was 25 ℃ and the humidity value was 30% [32].

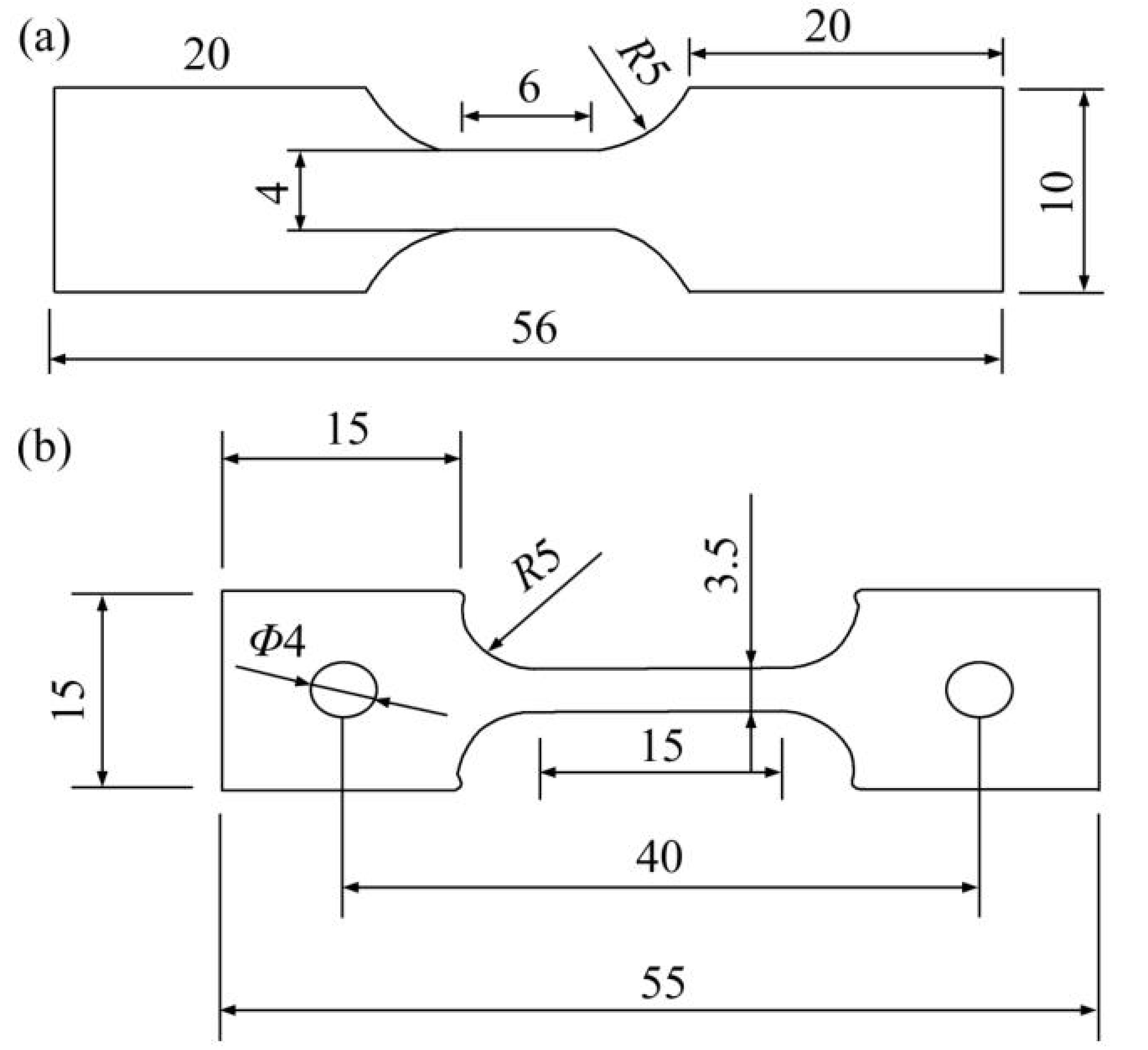

Figure 5 Schematic drawing of samples for (a) creep and (b) tensile tests (Unit: mm)

3 Results and discussion

3.1 Microstructure

The morphology of composite samples manufactured after eight cycles and with 5 wt% SiC_p is shown in Figure 6. As can be seen, there is a uniform dispersion of SiC_p through the metallic matrix demonstrating a desirable bonding between matrix and particles [33].

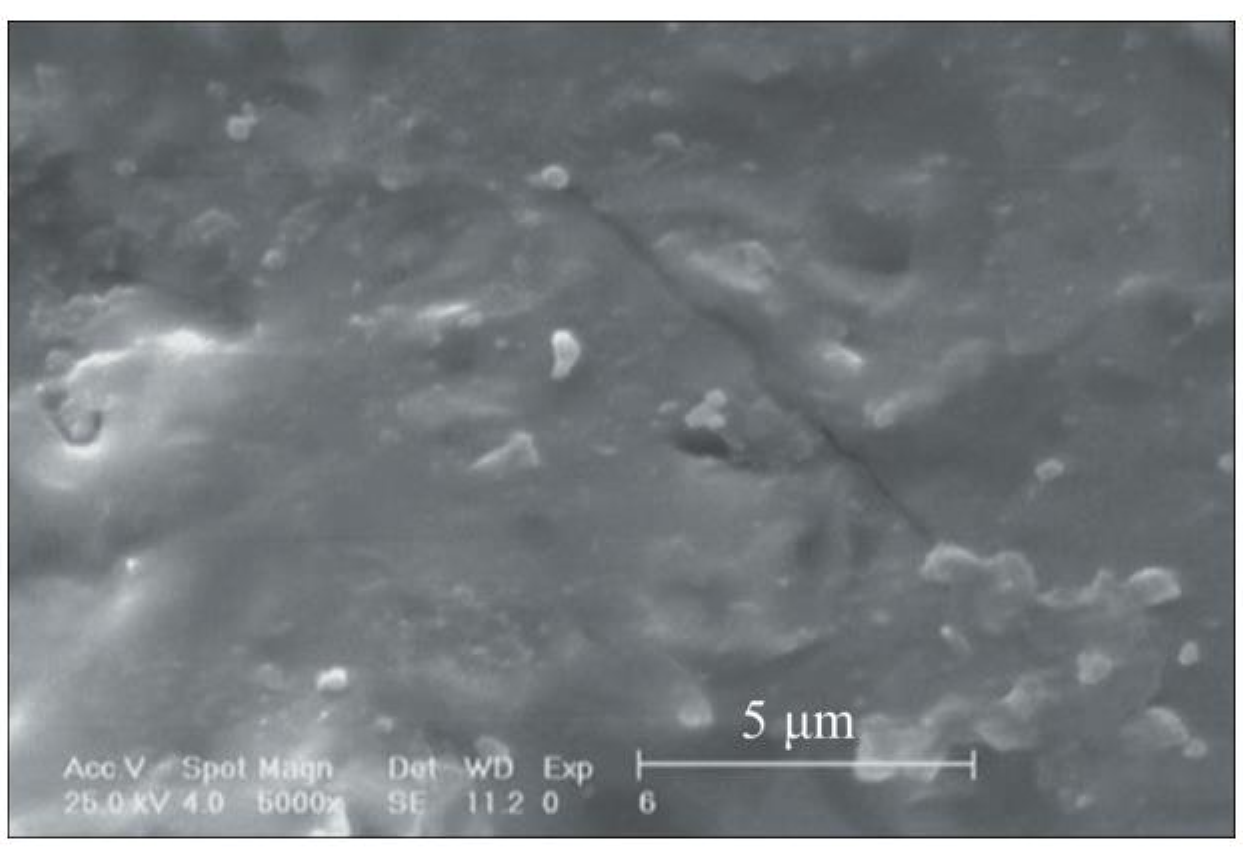

Figure 6 SEM surface morphology of Al/5 wt% SiC composites

After that, the bonding strength between Al and Cu layers is investigated in order to study the bonding mechanism. Based on the results obtained and owing to the higher strength of copper, the strain hardening of copper layers is more than Al alloy. So, the thinning phenomenon for both Al and Cu layers is the same due to the heterogeneous deformation, and the thickness of Cu layers begins to change at higher passes. Moreover, after each cycle, the Cu layer begins to neck in many areas with more distortion, as shown in Figure 7 [34−41].

Figure 8 shows the schematic illustration of the necking and rapture of Cu layers during the ARB process. As can be seen, Cu layers have tendency to break faster in higher cycles.

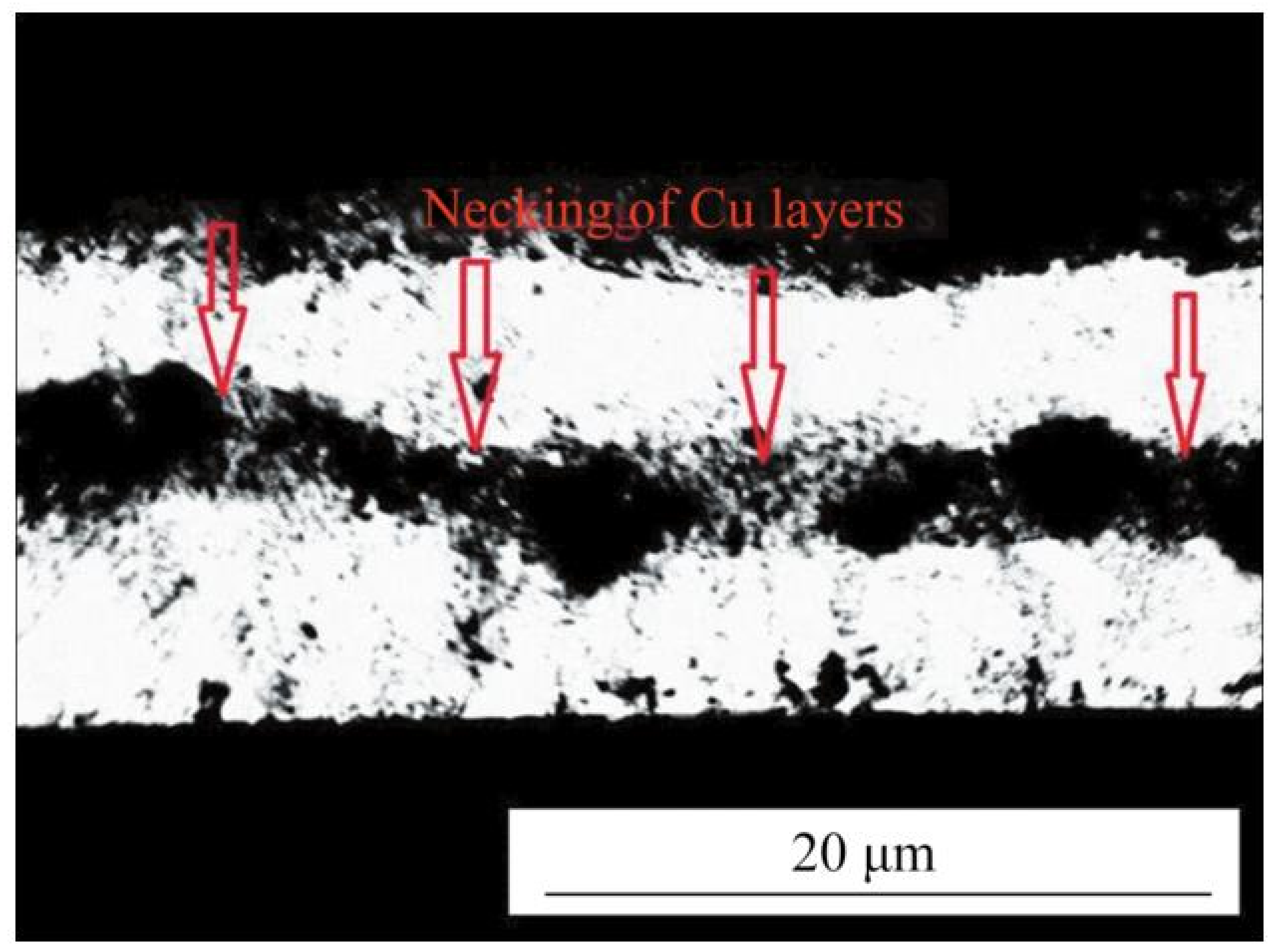

Figure 7 Necking of Cu layers after two cycles

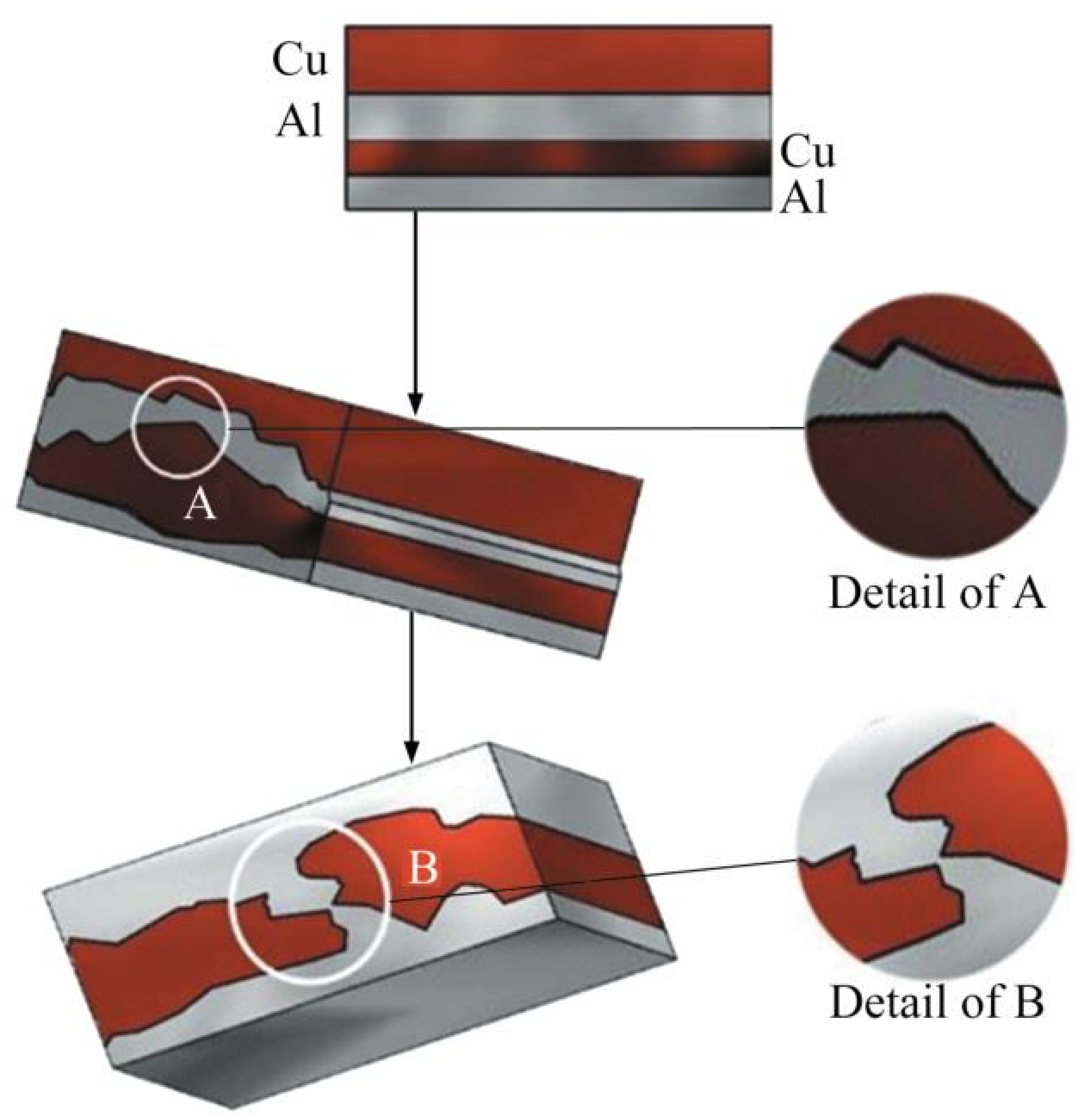

Figure 8 A schematic illustration of necking and rapture of Cu layers during ARB process

So, increasing stress and strain values of composite samples during the ARB process (specially at higher passes) leads to increasing tensile toughness value, as shown in Figure 8. Thus, growth in strain values and strength of the samples through the ARB process will increase according to Figure 8, the transplantation between Al and Cu dipping has happened with increasing pressure load.

For this reason, hardness increases gradually with prolonging the ARB process.

3.2 Creep properties

Figure 9 shows the composite sample fabricated with 2.5 wt% of SiC_p before and after the creep test. The effect of loading conditions is shown in Figure 10. As can be seen, the slope of creep curve increases for monolithic Al and composite sample with 7.5 wt% SiC_p in the second stage. This behavior can be contributed to the predominance of recovery over hard work. After the first stage, samples quickly enter the third stage by increasing the applied stress from 30 to 40 MPa at 250 °C. Instead of the lengthening of the second stage, the creep behavior of the 2.5 wt% SiC composite (at 250 °C stress of 30 MPa) shows the shortening of the first and third stages. According to Figure 10, at a constant temperature with no significant effect on the interface thickness, the stress level decreased by 13% and the creep failure time declined by 44%. Due to the prevention of slippage of the accumulated dislocations by addition of SiC_p, this behavior shows the establishment of a balance

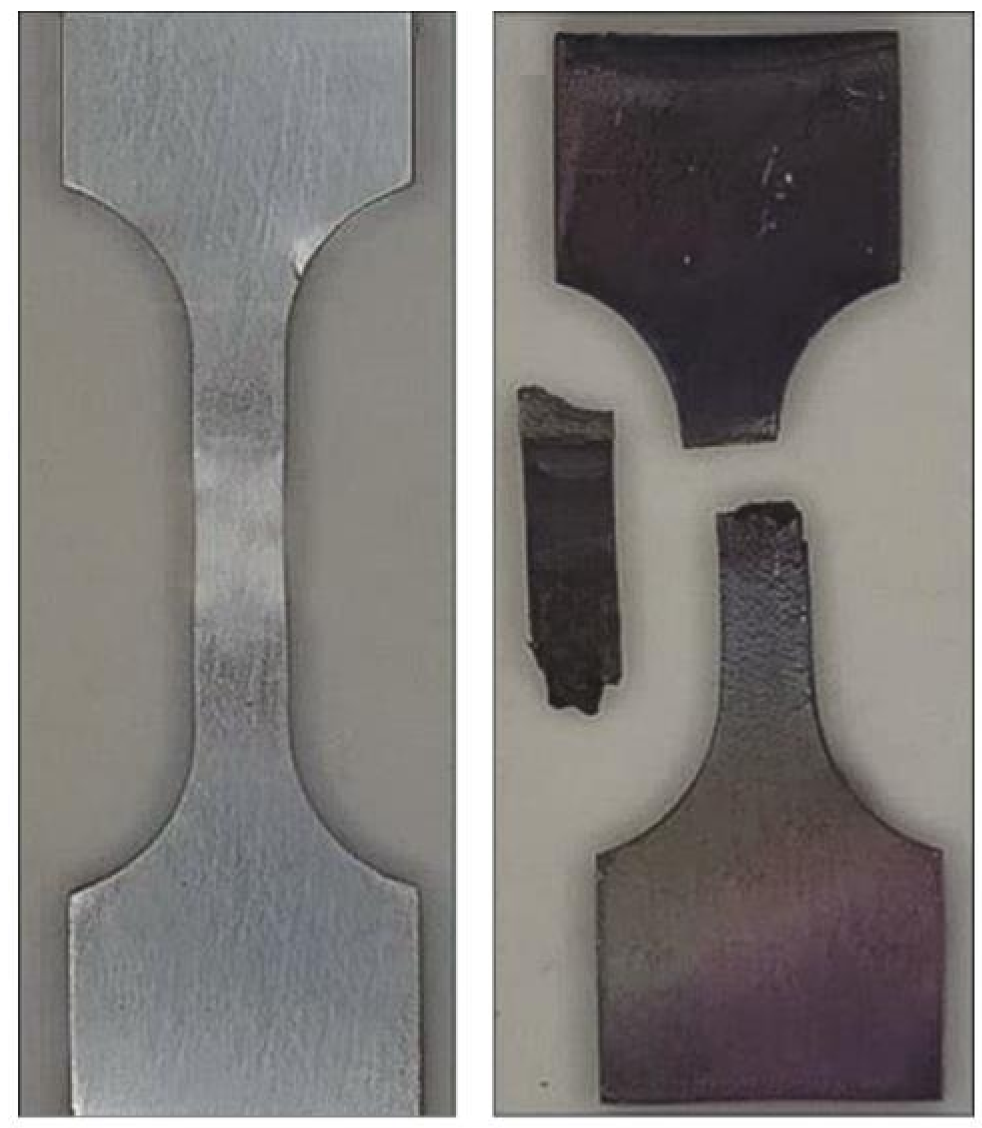

Figure 9 Al/2.5% SiC/Cu composites (a) before and (b) after the creep test

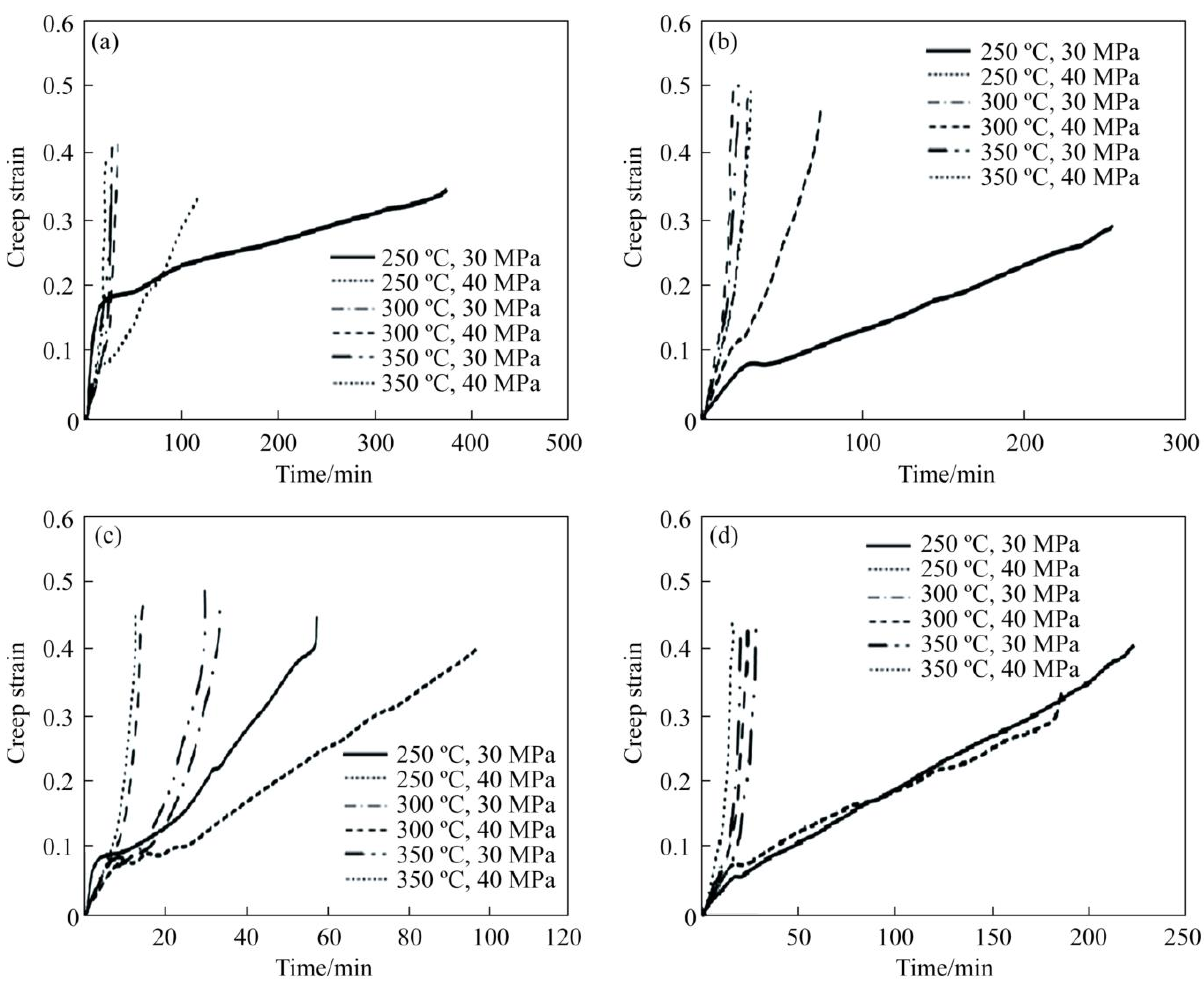

Figure 10 Creep strength of Al (a), and Al/SiC/Cu composites with 2.5% (b), 5% (c) and 7.5% (d) SiC particles for applied load and strength

between the workability and recovery. In other words, it causes a subsequent decrease for creep life of composites and a decrease in the second stage by increasing the stress to 40 MPa at the same temperature. In comparison with the monolithic sample, a uniform scattering of SiC_p can be cited as the reasons for its superior properties. So, higher SiC_p content has caused a decrease in the creep life compared to the annealed Al due to the large size of these particles and the lack of sufficient space for a more uniform distribution. Figure 11 illustrates a form of current situation. As can be seen in Figure 11, Al_2Cu deposits are present in all samples in an equal amount. The volume fraction of SiC_p in composite samples is the only parameter that can be controlled. So, the higher the applied stresses, the more the excreted pressure on SiC_p by dislocations. SiC_p cannot play a prominent role in preventing the movement of dislocations and the composite samples are recovered, which shortens the second stage of the creep phenomenon [34−37].

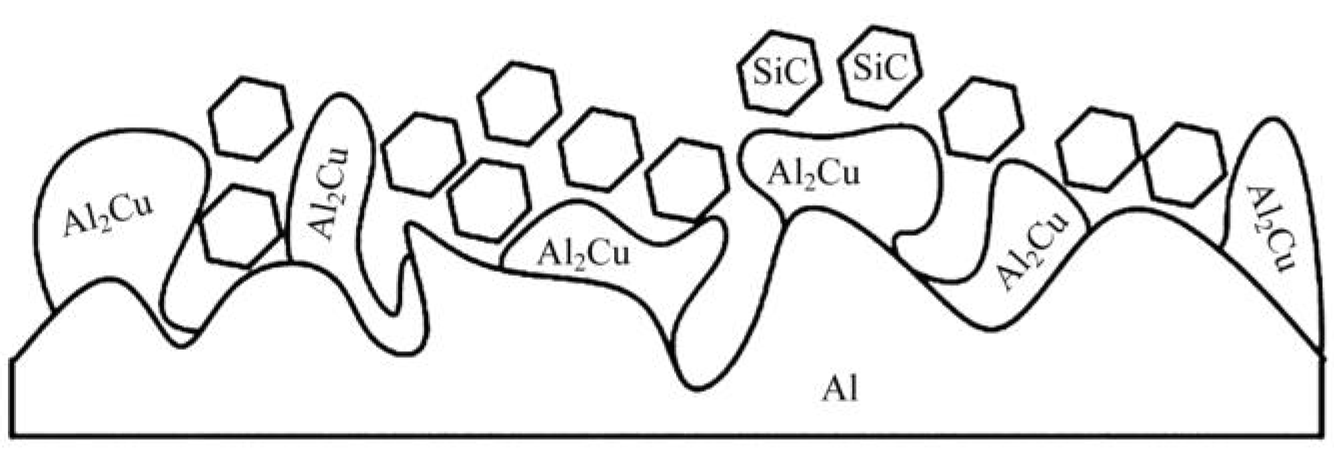

Figure 11 Schematic illustration of macroscopic diagrams of situation in composite samples

It is necessary to mention that in comparison with other samples, Al_2Cu deposits were present in the annealed Al which has a longer creep life. In the same way, increasing temperature from 250 to 350 °C at a stress of 40 MPa has caused complete elimination of the second stage and rapid entry of this sample into the third stage, which severely reduces the creep life. The activation of multiple sliding systems and misplaced sliding can be considered as the main reason for the occurrences of these phenomena. In other words, the locking effect of SiC_p at higher ratios of SiC_p in the grain boundaries improves the creep resistance and weakens the creep resistance.

3.3 Unaxial tensile properties

Figure 12 illustrates the stress−strain curve of Al/SiC/Cu composites with 5 wt% SiC using a

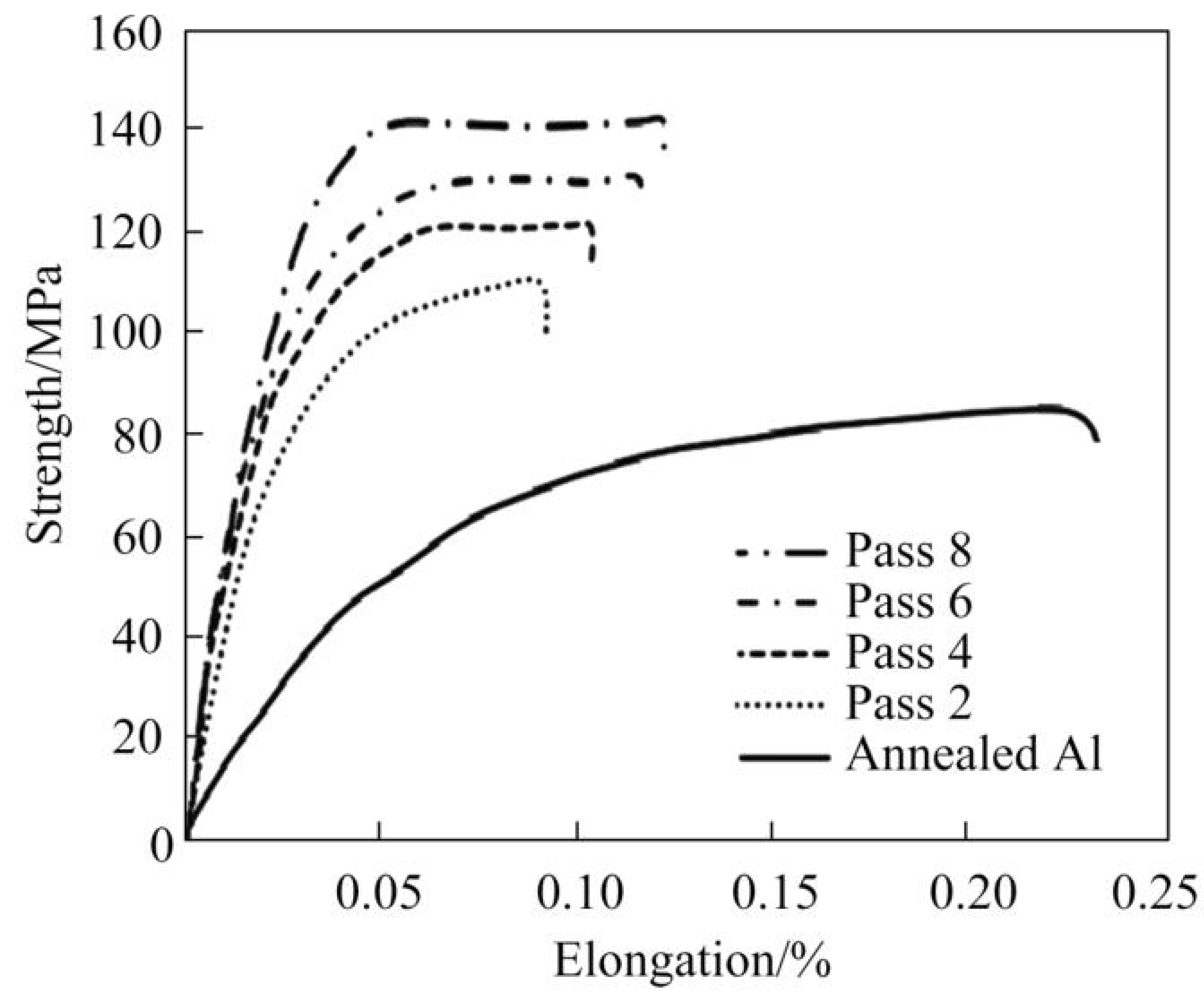

Figure 12 Stress−strain diagram of Al/SiC/Cu laminated composite

uniaxial tensile test. As can be seen in Figure 12, ARB has a positive effect on the improvement of stress and strain amplitudes at higher passes. Dislocations strengthening and less mobility of dislocation lead to improvement of the tensile strength [32]. The improvement of strength is due to dislocation strengthening, less mobility of dislocation, the failure of harder Cu phase and its scattering inside the soften Al matrix, and also local strain hardening of metallic matrix around SiC_p. According to Figures 6 and 7, bonding strength debilitates due to the increased stress. So, the rapture of Cu layers endures slight plastic deformation due to the higher strength of Cu. Moreover, a wide span is shaped in the stress−strain curve as a result of the ductile fracture of Al. The enhancement of the elongation value can be attributed to the increasing of the bonding between layers, the dynamic recrystallization at higher cycles, the uniform scattering of SiC_p by breaking of particles agglomerations at higher cycles and then, the enhancement of the bonding strength between Al and Cu layers.

3.4 Hardness

The Vickers micro hardness (HV) for Al is HV (52.08±2.29) and for Cu is HV (100±2.74). Also, the interface of micro hardness in laminated metal composite are HV (114.83±2.41), HV (62.3±2.36), and HV (123.7±2.95) for Cu and Al, respectively. Cu exhibits more hardness value than Al due to its high work hardening ability. Noticeably, both Al and Cu show increased hardness due to induced work hardening effect. But, this region demonstrates a higher hardness level. Other governing factors on the improvement of micro hardness are different in thermo physical properties between Al and Cu, and residual stresses of ARB process.

3.5 Creep behavior

Figure 13 illustrates the variations for strain and time during the creep test for samples which were conducted under several stresses and temperatures: (a) 35 MPa/225 °C, (b) 35 MPa/275 °C, and (c) 30 MPa/225 °C. Each creep curve includes three steps from the first step up to the third step.

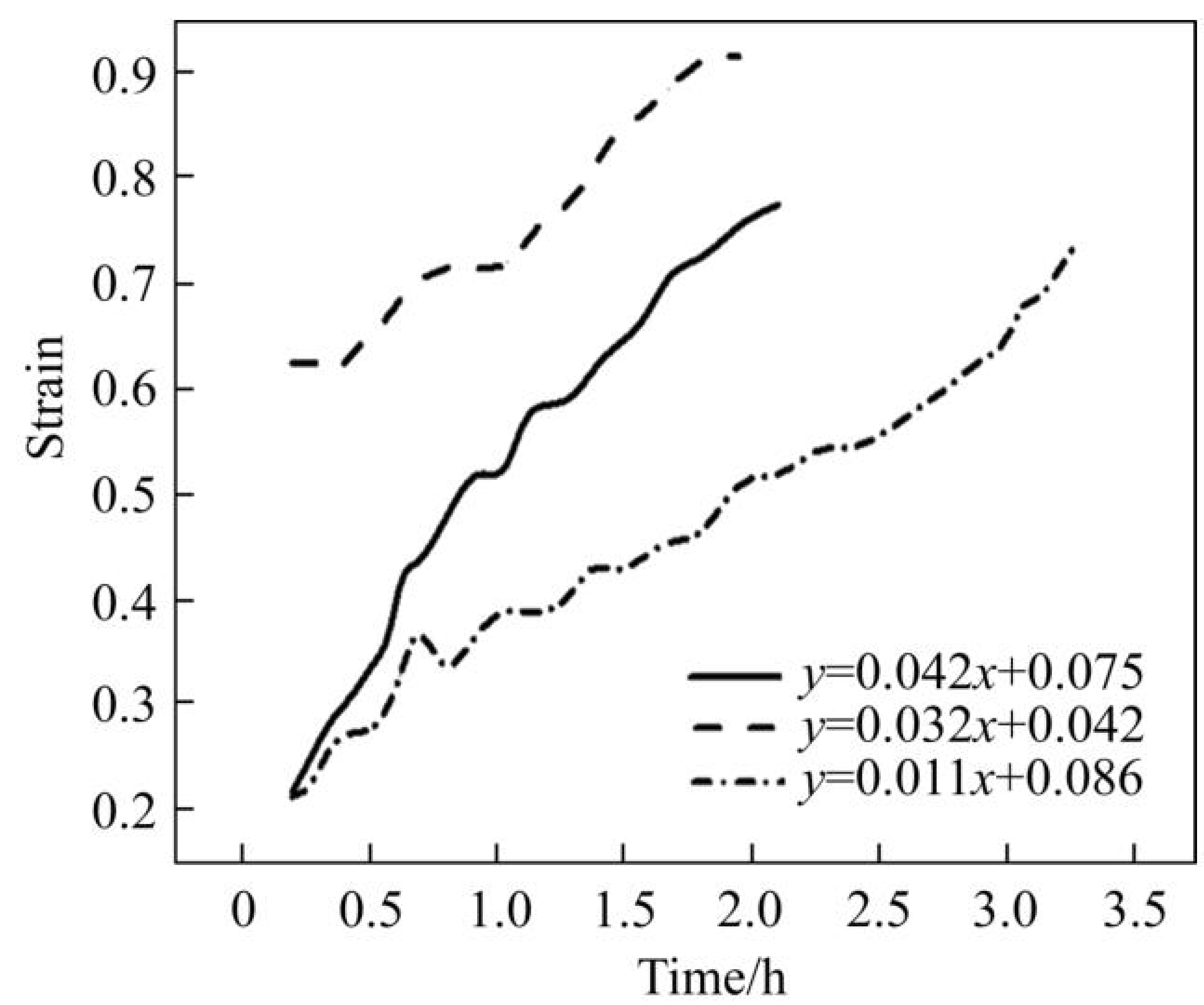

Figure 13 Effect of applied loading conditions on slope of secondary creep curves

For the first creep stage, line slope drops severely after rolling which leads to increasing the creep resistance due to severe strain hardening. During the second stage, the strain rate remains constant with a fair estimate considering thermal recovery and strain hardening, which shows a linear trend for the creep curve. Roughly balanced work hardening and softening lead to the occurrence of this stage. So, necking and severe stress acceleration lead to the reduction of cross sections. Furthermore, the composite sample ruptures at higher strain rates. The effect of loading conditions on the variations of the creep strains is shown in Figure 13. The specifications for each stage is illustrated in Table 1.

High values of elongation during the creep test leads to increased temperature which makes a brittle matrix. This brittle metallic matrix drops the strength and elongation values. Figure 13 and Table 2 show the slope values of creep curves under different loading conditions. As can be seen, the second slope of the creep curve reached to 39% with an increase in the stress level at constant temperature. Then, it drops to 2% with a little temperature rising. So, creep constitutive models have been developed to predict time-dependent deformation.

Norton's power law as the most significant equation is shown as:

$$\dot{\varepsilon}_{cr}=\frac{d\varepsilon_{cr}}{dt}=A\sigma^{B}e^{\frac{-C}{T}} \tag{1}$$

where A, B and C are coefficients; $\frac{d\varepsilon_{cr}}{dt}$ is the creep strain rate; T is the applied temperature; r is the testing stress.

Figures 14 and 15 illustrate that the approximation of creep performance of samples has been obtained by drawing the stresses and temperature as input and strain rate as output, respectively.

3.6 Evolution of microstructural morphology

Figure 16 shows the SEM morphology of samples along the rolling direction. As shown, no evident intermetallic compound is seen along the straight interface, which is reported in other studies [31]. A brittle interface can negatively affect the bonding strength and mechanical properties. So,

Table 1 Strain and time values during creep test

Loading condition	Stage 1		Stage 2		Stage 3	
	Strain/%	Time/h	Strain/%	Time/h	Strain/%	Time/h
30 MPa at 225 °C	0.23±0.15	2.70±0.14	4.13±0.14	5.40±0.24	0.63±0.16	8.49±0.45
35 MPa at 225 °C	0.34±0.07	2.20±0.19	1.42±0.17	8.20±0.13	0.61±0.03	11.20±0.33
35 MPa at 275 °C	0.17±0.04	5.20±0.22	1.13±0.11	9.12±0.32	0.27±0.14	12.72±0.22

Table 2 Slope of secondary creep curve linear equation vs loading conditions

Creep loading condition	Line equation	Slope/(°)
35 MPa at 275 °C	$y=0.042x+0.075$	74.32
35 MPa at 225 °C	$y=0.032x+0.042$	76.34
30 MPa at 225 °C	$y=0.011x+0.086$	57.91

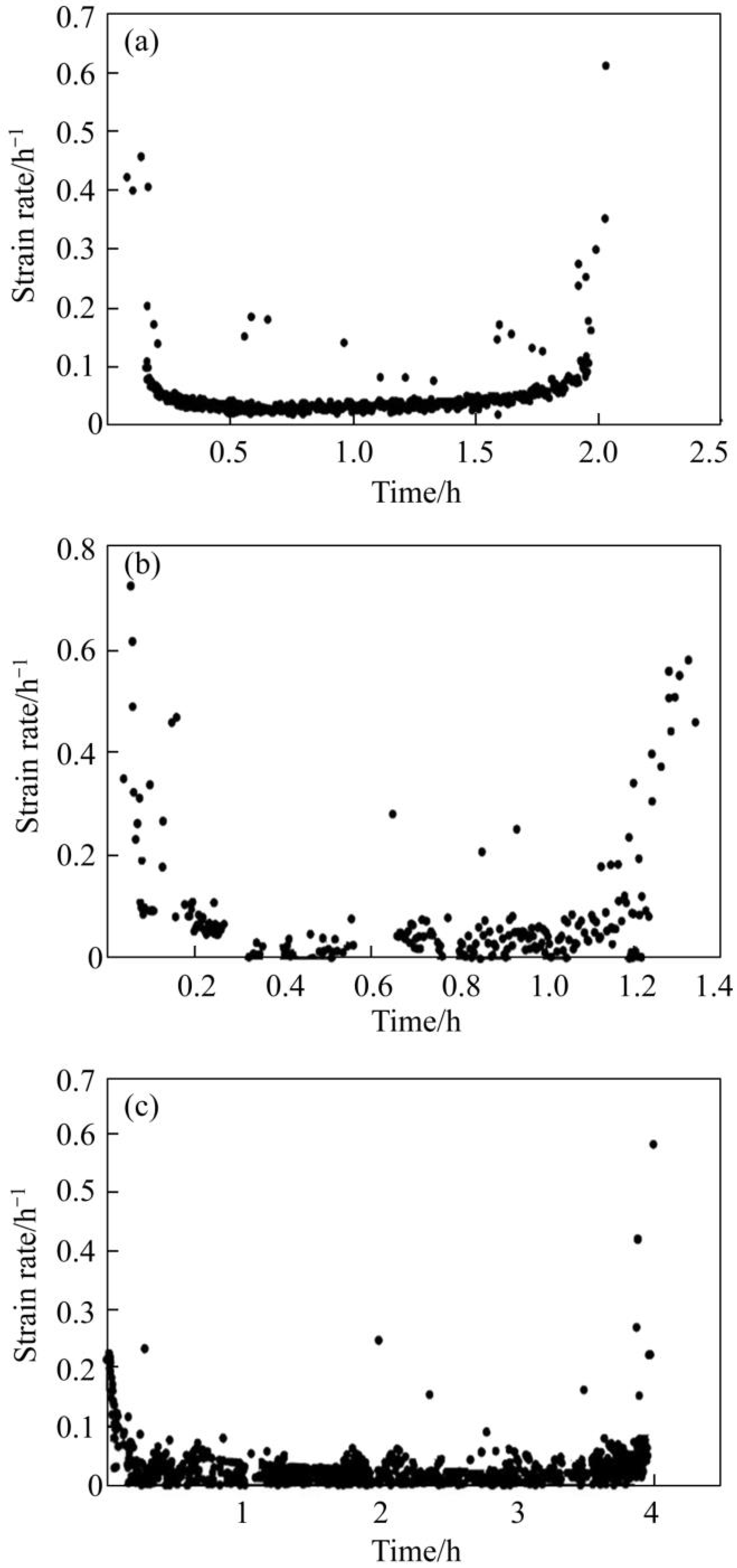

Figure 14 Creep strain for samples: (a) 35 MPa 225 °C; (b) 35 MPa at 275 °C; (c) 30 MPa at 225 °C

intermetallic phases don't demonstrate a desirable bonding between Al and Cu layers during the roll bonding. So, no noticeable variations of SiC_p scattering have been observed along the interface. The slope of X-shaped curve indicates the atomic

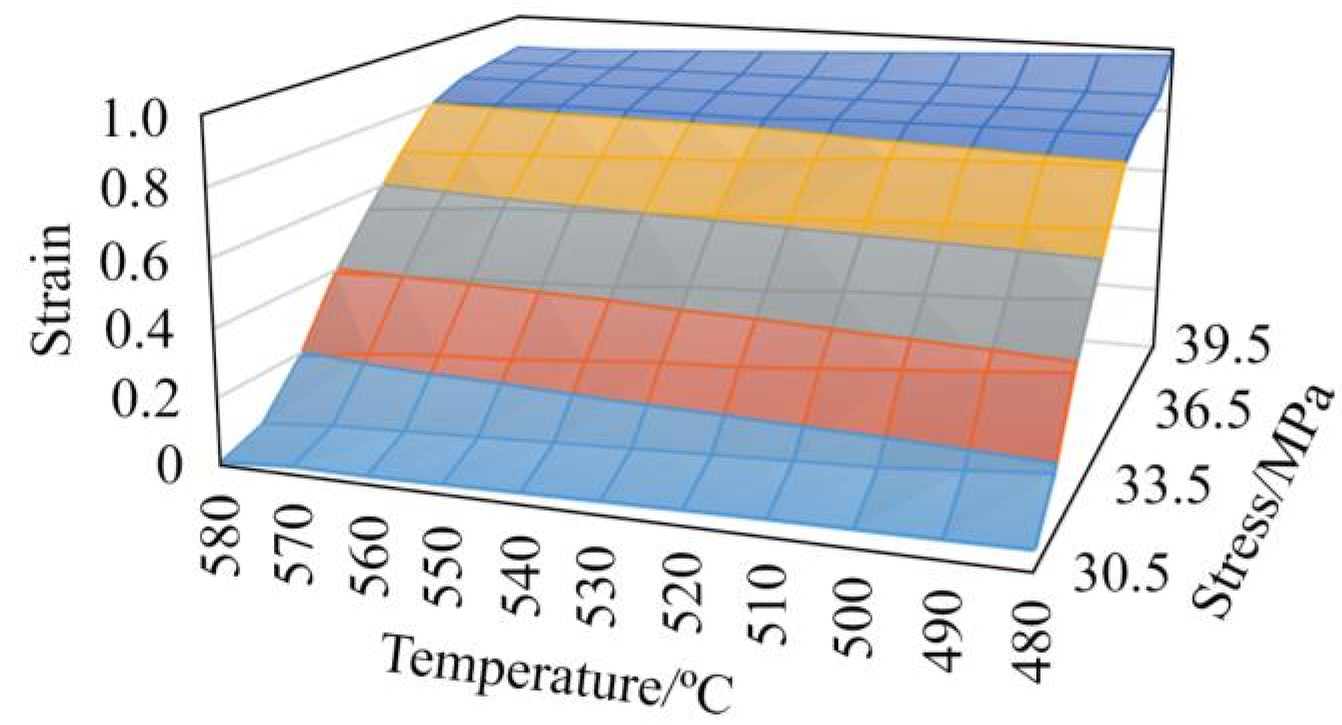

Figure 15 Surface creep trend of Al/SiC/Cu composite samples

diffusion along the bonding interface. The optimal microscopy (OM) images of samples is shown in Figure 17, tiny grains near the interface aligned along the rolling direction. Furthermore, a heterogeneous graining scattering in the Cu layer containing tiny grains near the interface and coarser grains further away from the boundary can be seen. The recrystallization of ARB process leads to generation of this behavior which changes the grains form from stretched to an equiaxed style.

Figure 18 illustrates the spreading of Al and Cu in the thickness direction around the interface, and lists the composition taken from EDX analysis from points A to B, showing a decrease in Cu and an increase in Al, respectively.

3.7 Effect of creep loading on microstructural evolution

Figure 19 shows the effect of creep loading conditions on the SEM morphologies of composite samples. As can be seen, when exposed to elevated temperatures and stress levels under creep loadings, the interface thickness increases by 40% due to the activation of diffusion in this state. So, the interface decreases by 15.6% by reducing the fracture time with higher stress levels. The results for the composite under creep test conditions (30 and 35 MPa at 225 °C) demonstrated that no intermetallic composition has formed at the interface. But, intermetallic compounds were observed for creep test conditions of 35 MPa at 275 °C. Figure 19 shows the point used in the EDS pointer analysis. As the shift from Al to Cu occurs, the amount of aluminum decreases and its spreading becomes more distributed. So, its scattering

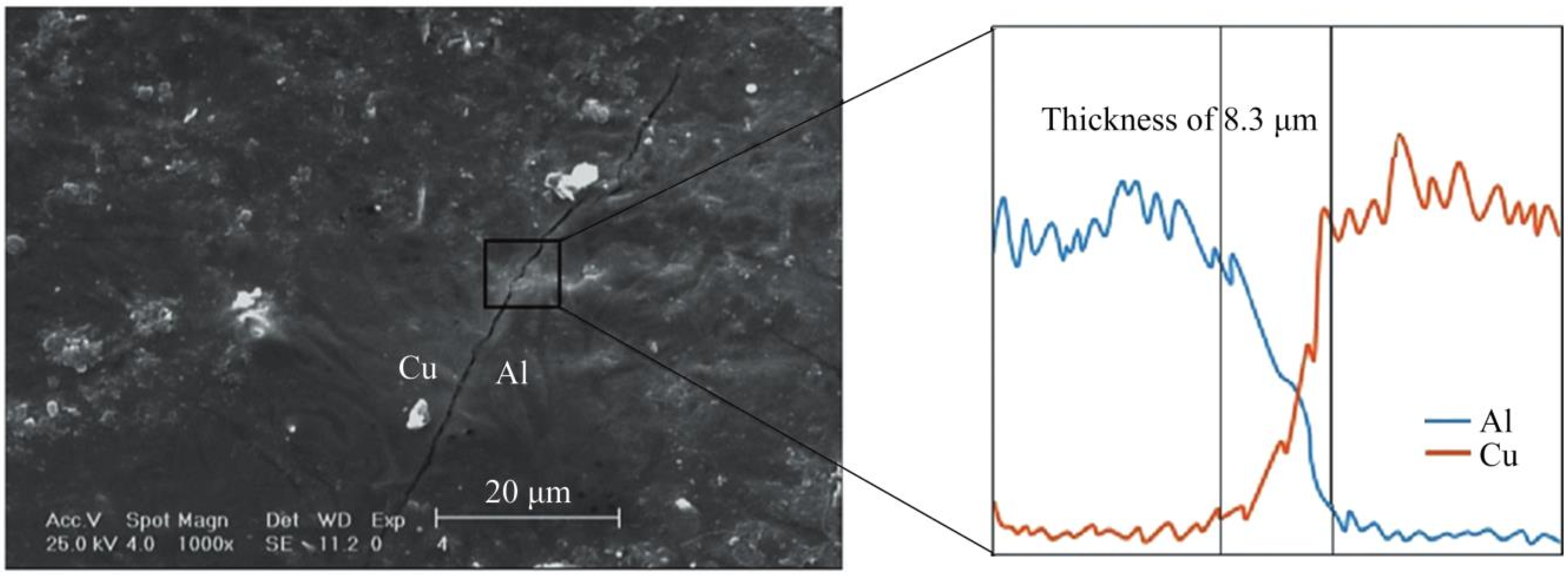

Figure 16 SEM cross section analysis of Al/SiC/Cu composites

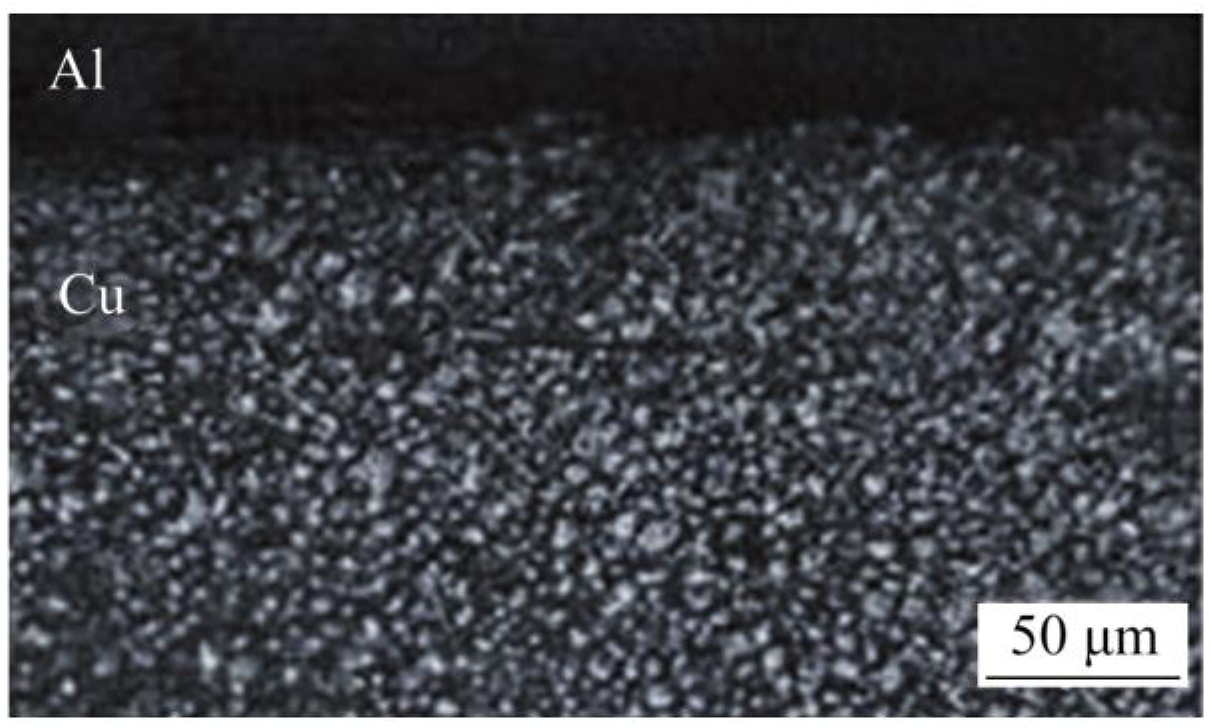

Figure 17 OM microstructural morphology of Cu layer

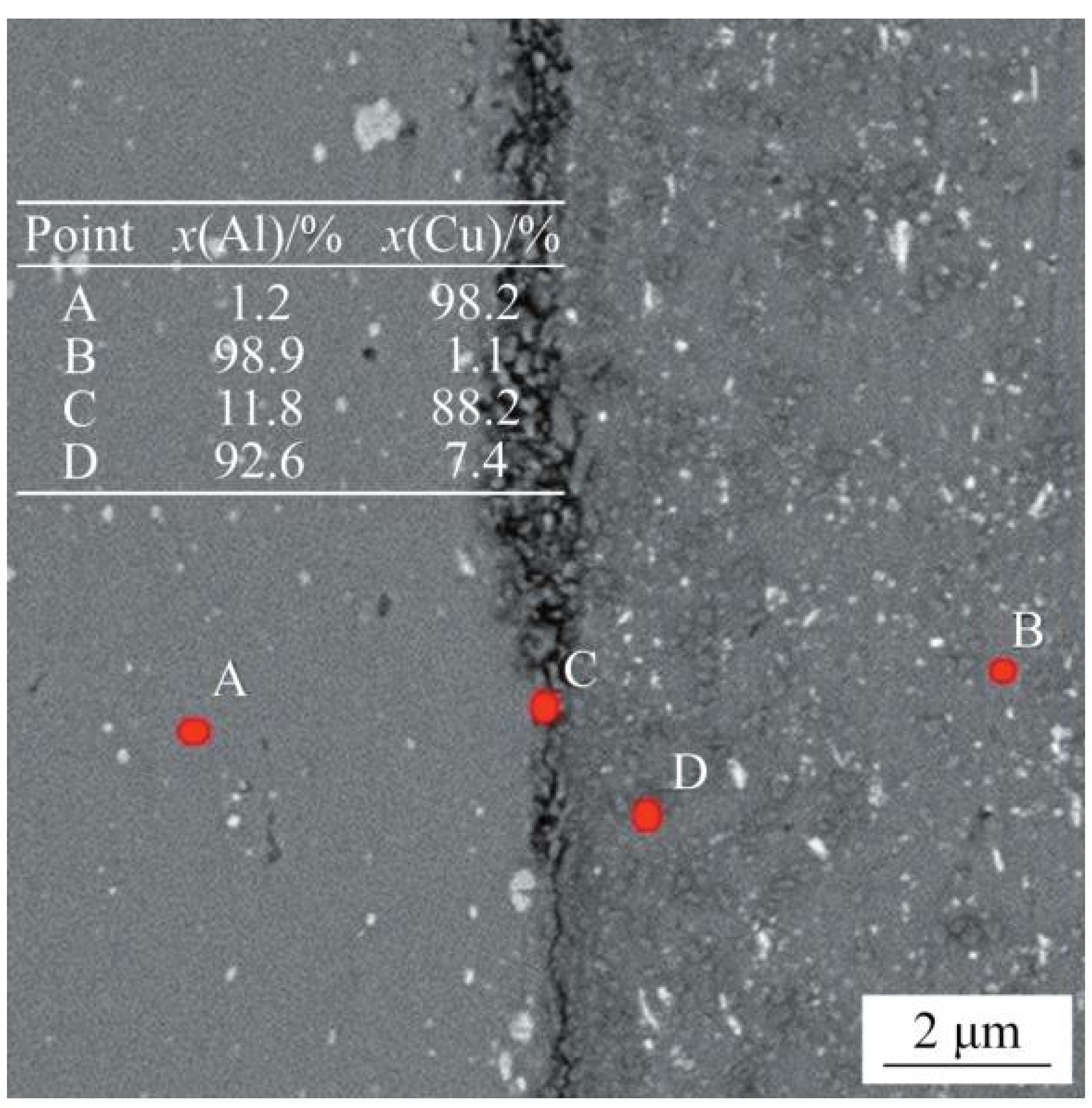

Figure 18 EDS analysis of composite sample

converts more unvarying at higher values of Cu. The Al to Cu ratio at point C indicates the existence of Al_2Cu where intermetallic compositions were shaped. The microstructure of copper at a temperature of 275 °C and under a loading of 35 MPa is shown in Figure 19. As can be seen, no intermetallic compound is observed around the interface, meaning an atomic diffusion between Al and Cu. Furthermore, the composite sample under creep conditions (30 MPa at 225 °C) shows a more unvarying grain scattering (Figure 20(c)).

4 Conclusions

In this study, ARB process is used to fabricate bimetal Al/Cu composite strips. The effect of creep loading conditions (stress and temperature) has been investigated on the mechanical, bonding, microstructural, and creep properties of Al/SiC/Cu composites samples. The following results can be concluded.

1) Two drops can be found in the creep curves due to the fracture of Al and Cu layers. Moreover, formation of solid solution leads to improvement of the hardness.

2) The accumulation of dislocations during the cumulative rolling process can be considered as one of the main reasons for the hardness enhancement.

3) The creep life of Al/2.5%SiC/Cu composite is measured at all temperatures and strain rates more than other manufactured composites.

4) The interface thickness increases by 40% which leads to the formation of intermetallic compounds in this region when the temperature increases with a constant stress.

5) Two main affecting parameters on the creep strain are stress and temperature. It is observed that while the temperature is constant in different conditions, the second slope of the creep curve reaches to 39% with an increase in the stress level. Then, it drops to 2% with a little temperature rising.

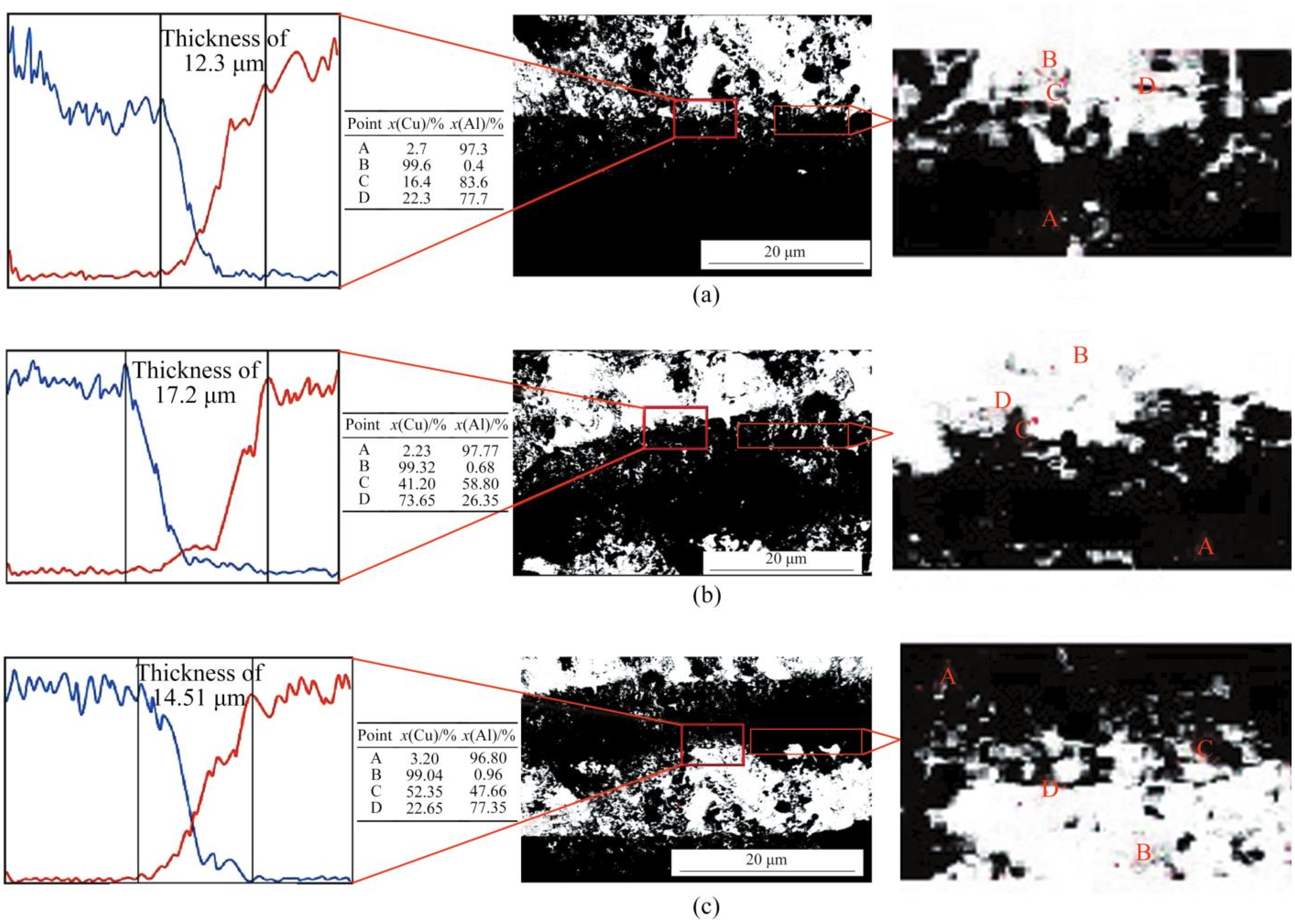

Figure 19 Effect of creep loading conditions: (a) 35 MPa at 225 °C; (b) 35 MPa at 275 °C; (c) 30 MPa at 225 °C

6) The sample after creep test at 275 °C/ 35 MPa displays the presence of 60% Al and 40% Cu, containing brittle Al_2Cu intermetallic compound at the interface.

Contributors

Basem Ali, Jasim Dheyaa J. and Brisset BJ. provided the concept and edited the draft of manuscript. Bansal Pooja and Brisset BJ. conducted the literature review and wrote the first draft of the manuscript. Qasim Maytham T. edited the draft of manuscript.

Conflict of interest

BASEM Ali, Jasim Dheyaa J., Bansal Pooja, Qasim Maytham T. and Brisset BJ. declare that they have no conflict of interest.

References

[1] ZHANG Gui-feng, WANG Xin-wei, CHENG Ruo-liang, et al. Fabricating surface composite by friction stir brazing SiCp/A356 composite sheet onto monolithic Al plate in air [J]. Journal of Materials Engineering and Performance, 2024, 33(2): 819−830. DOI: 10.1007/s11665-023-08036-8.

[2] BAGHERI B, ABBASI M, SHARIFI F, et al. Different attempt to improve friction stir brazing: Effect of mechanical vibration and rotational speed [J]. Metals and Materials International, 2022, 28(9): 2239−2251. DOI: 10.1007/s12540-021-01121-4.

[3] SHANG Meng-ya, MIAO Wei, JIA Dong-qing, et al. Fabrication and characterization of PMMA/MWCNTs composite materials [J]. Journal of Wuhan University of Technology-Materials Science Edition, 2023, 38: 1190−1197. DOI: 10.1007/s11595-023-2809-y.

[4] LI Mei-juan, CHENG Ping, LIU Cheng, et al. Effect of graphene surface functional groups on the mechanical property of PMMA microcellular composite foams [J]. Journal of Wuhan University of Technology-Mater Sci Ed, 2019, 34(3): 717−722. DOI: 10.1007/s11595-019-2108-9.

[5] RADHY N, JASIM L. A novel economical friendly treatment approach: Composite hydrogels [J]. Caspian Journal of Environmental Sciences. 2019, 19(5): 841−852. DOI: 10.22124/cjes.2021.5233.

[6] GAO Y, VINI M H, DANESHMAND S. Effect of nano Al_2O_3 particles on the mechanical and wear properties of Al/Al_2O_3 composites manufactured via ARB [J]. Reviews on Advanced Materials Science, 2022, 61(1): 734−743. DOI: 10.1515/rams-2022-0268.

[7] SAMADI MOLLAYOUSEFI H, FALLAH SHOJAEI A, MAHMOODI N. Preparation, characterization, and performance study of pvdf nanocomposite contained hybrid nanostructure TiO_2-POM used as a photocatalytic membrane [J]. Iranian Journal of Chemistry and Chemical Engineering, 2021, 40(1): 35−47. DOI: 10.22124/CJES.2021. 5233.

[8] NAEIMI A, NEJAT R. Synthesis and characterization of a novel bio-magnetically recoverable palladium nanocomposite for the photocatalytic applications [J]. Iranian Journal of Chemistry and Chemical Engineering, 2022, 41(1): 15−26. DOI: 10.30492/ijcce.2021.121648.3975.

[9] AHMED KHAN I, HUSSAIN H, YASIN T. Fabrication and characterization of amidoxime-grafted silica composite particles via emulsion graft polymerization [J]. Iranian Journal of Chemistry and Chemical Engineering, 2020, 39(5): 111−120. DOI: 10.30492/ijcce.2020.39789.

[10] ADIN H, ADIN M Ş. Effect of particles on tensile and bending properties of jute epoxy composites [J]. Materials Testing, 2022, 64(3): 401−411. DOI: 10.1515/mt-2021-2038.

[11] TAYYEBI M, RAHMATABADI D, KARIMI A, et al. Investigation of annealing treatment on the interfacial and mechanical properties of Al5052/Cu multilayered composites subjected to ARB process [J]. Journal of Alloys and Compounds, 2021, 871: 159513. DOI: 10.1016/j. jallcom. 2021.159513.

[12] TAYYEBI M, RAHMATABADI D, ADHAMI M, et al. Influence of ARB technique on the microstructural, mechanical and fracture properties of the multilayered Al1050/Al5052 composite reinforced by SiC particles [J]. Journal of Materials Research and Technology, 2019 , 8(5): 4287−4301. DOI: 10.1016/j.jmrt.2019.07.039.

[13] RAHMATABADI D, TAYYEBI M, NAJAFIZADEH N, et al. The influence of post-annealing and ultrasonic vibration on the formability of multilayered Al5052/MgAZ31B composite [J]. Materials Science and Technology, 2021, 37(1): 78−85. DOI: 10.1080/02670836.2020.1867784.

[14] GHASEMVAND M, BEHJAT B, EBRAHIMI S. Experimental investigation of the effects of adhesive defects on the strength and creep behavior of single-lap adhesive joints at various temperatures [J]. The Journal of Adhesion, 2023, 99(7): 1227 − 1243. DOI: 10.1080/00218464.2022.20 95262.

[15] MARCHENKO E, BAIGONAKOVA G, KOKOREV O, et al. Phase equilibrium, structure, mechanical and biocompatible properties of TiNi-based alloy with silver [J]. Materials Research Express, 2019, 6(6): 066559. DOI: 10. 1088/2053-1591/ab0edd.

[16] DUN Dong-xing , LUO Jing-yun, WANG Ming-hao, et al. Electromagnetic interference shielding foams based on poly (vinylidene fluoride)/carbon nanotubes composite [J]. Macromolecular Materials and Engineering, 2021, 306(12): 2100468. DOI: 10.1002/mame.202100468.

[17] WANG Sai, HUANG Yi-feng, CHANG E, et al. Evaluation and modeling of electrical conductivity in conductive polymer nanocomposite foams with multiwalled carbon nanotube networks [J]. Chemical Engineering Journal, 2021, 411: 128382. DOI: 10.1016/j.cej.2020.128382.

[18] MOJTAHEDI A, HOKMABADY H, KOUHI M, et al. A novel ANN-RDT approach for damage detection of a composite panel employing contact and non-contact measuring data [J]. Composite Structures, 2022, 279: 114794. DOI: 10.1016/j.compstruct.2021.114794.

[19] GHOLAMI M D, SALAMAT M, HASHEMI R. Study of mechanical properties and wear resistance of Al 1050/brass (70/30)/Al 1050 composite sheets fabricated by the accumulative roll bonding process [J]. Journal of Manufacturing Processes, 2021, 71: 407−416. DOI: 10.1016/ j.jmapro.2021.09.032.

[20] CHAMBERS C, PROCTOR C, KABLER P. Bactericidal effects of low concentrations of silver [J]. Journal American Waterworks Association, 1962, 54: 206−216. DOI: 10.1002/ j.1551-8833.1962.tb00834.x.

[21] ROUZBEH A, HASHEMI R, SEDIGHI M. Experimental and numerical study of microstructure, mechanical characteristics, and forming limit curve for Al_{1050}/Mg-AZ31B two-layer sheets manufactured via roll bonding technique [J]. Journal of Alloys and Compounds, 2023, 942: 169059. DOI: 10.1016/j.jallcom.2023.169059.

[22] WANG Wei-ning, HEYDARI VINI M, DANESHMAND S. Mechanical and wear properties of Al/TiC composites fabricated via combined compo-casting and APB process [J]. Crystals, 2022, 12(10): 1440. DOI: 10.3390/cryst12101440.

[23] LV Xue-qi, WU Chuan-song, YANG Chun-liang, et al. Weld microstructure and mechanical properties in ultrasonic enhanced friction stir welding of Al alloy to Mg alloy [J]. Journal of Materials Processing Technology, 2018, 254: 145−157. DOI: 10.1016/j.jmatprotec.2017.11.031.

[24] ROUZBEH A, SEDIGHI M, HASHEMI R. Effects of strain path on the microstructure, tensile properties, and formability of Al/Mg roll-bonded sheets [J]. Journal of Materials Research and Technology, 2023, 23: 5318 − 5328. DOI: 10. 1016/j.jmrt.2023.02.148.

[25] ATIFEH S M, ROUZBEH A, SEDIGHI M, et al. Effect of rolling process on formability and mechanical properties of AA 1050/Mg AZ31B bilayer sheet [J]. Journal of Materials Engineering and Performance, 2023, 32(18): 8493 − 8502. DOI: 10.1007/s11665-022-07732-1.

[26] CHEN Shu-jun, JIANG Xiao-qing. Microstructure evolution during magnetic pulse welding of dissimilar aluminium and magnesium alloys [J]. Journal of Manufacturing Processes, 2015, 19: 14−21. DOI: 10.1016/j.jmapro.2015.04.001.

[27] LUO Chang-zeng, LIANG Wei, CHEN Zhi-qiang, et al. Effect of high temperature annealing and subsequent hot rolling on microstructural evolution at the bond-interface of Al/Mg/Al alloy laminated composites [J]. Materials Characterization, 2013, 84: 34 − 40. DOI: 10.1016/j. matchar. 2013.07.007.

[28] NIE Hui-hui, LIANG Wei, CHEN Hong-sheng, et al. Effect of annealing on the microstructures and mechanical properties of Al/Mg/Al laminates [J]. Materials Science and Engineering A, 2018, 732: 6 − 13. DOI: 10.1016/j. msea. 2018.06.065.

[29] USCINOWICZ R. The effect of rolling direction on the creep process of Al-Cu bimetallic sheet [J]. Materials & Design, 2013, 49: 693 − 700. DOI: 10.1016/j. matdes. 2013. 02.012.

[30] AVALLONE J T, NIZOLEK T J, BALES B B, et al. Creep resistance of bulk copper − niobium composites: An inverse

effect of multilayer length scale [J]. Acta Materialia, 2019, 176: 189−198. DOI: 10.1016/j.actamat.2019.06.029.
[31] USCINOWICZ R. Creep of a laminated aluminum-zinc composite [J]. Materials Science, 2008, 44(2): 283 − 289. DOI: 10.1007/s11003-008-9069-z.
[32] TSAI H C, WOLFENSTINE J, SHERBY O D. Elevated temperature mechanical behaviour of an ultrahigh carbon steel/brass laminated composite [J]. Composites, 1991, 22(5): 373−379. DOI: 10.1016/0010-4361(91)90552-r.
[33] RACHID H B, NOUREDDINE D, BENALI B, et al. Effect of nanocomposites rate on the crack propagation in the adhesive of single lap joint subjected to tension [J]. Mechanics of Advanced Materials and Structures, 2023: 6898−6906. DOI: 10.1080/15376494.2023.2240319.
[34] RAISIE F, SEDIGHI M, ROUZBEH A. An experimental study on the creep behavior of Al1050/Mg AZ31B bilayer sheet fabricated via roll bonding [J]. Journal of Materials Engineering and Performance, 2023. DOI: 10.1007/s11665-023-08819-z.
[35] MACWAN A, JIANG X Q, LI C, et al. Effect of annealing on interface microstructures and tensile properties of rolled Al/Mg/Al tri-layer clad sheets [J]. Materials Science and Engineering A, 2013, 587: 344 − 351. DOI: 10.1016/j.msea.2013.09.002.
[36] LEE K S, YOON D H, KIM H K, et al. Effect of annealing on the interface microstructure and mechanical properties of a STS-Al-Mg 3-ply clad sheet [J]. Materials Science and Engineering A, 2012, 556: 319 − 330. DOI: 10.1016/j.msea.2012.06.094.
[37] ROUZBEH A, SEDIGHI M, HASHEMI R. Comparison between explosive welding and roll-bonding processes of AA1050/Mg AZ31B bilayer composite sheets considering microstructure and mechanical properties [J]. Journal of Materials Engineering and Performance, 2020, 29(10): 6322−6332. DOI: 10.1007/s11665-020-05126-9.
[38] ANNE G, RAMESH M R, NAYAKA H S, et al. Microstructure, mechanical and corrosion properties of accumulative roll bonded Mg-2%Zn/anodized Al-7075 composite [J]. Materials Today: Proceedings, 2018, 5(2): 6868−6877. DOI: 10.1016/j.matpr.2017.11.348.
[39] ADIN M Ş, KILIÇKAP E. Strength of double-reinforced adhesive joints [J]. Materials Testing, 2021, 63(2): 176−181. DOI: 10.1515/mt-2020-0024.
[40] DAI Jing-ru, WANG Yan-gang, GRANT T, et al. Low-temperature die attachment by pressureless Cu sintering for semiconductor packaging [J]. Journal of Electronic Materials, 2023, 52(11): 7607 − 7613. DOI: 10.1007/s11664-023-10656-8.
[41] FENG Xiao-wei, LI Jia-xin, ZHENG Zhi-bin, et al. Mechanical properties and fracture mechanism of Fe/Cu composite sheets with Al interlayer after annealing treatment [J]. Journal of Iron and Steel Research International, 2023, 30(9): 1888−1895. DOI: 10.1007/s42243-023-00958-w.

(Edited by FANG Jing-hua)

中文导读

通过累积轧制工艺制备的Al/SiC/Cu双金属复合材料的蠕变性能

摘要：本文研究了通过累积辊压结合(ARB)工艺制备的Al/SiC/Cu复合带材的微观结构演变、力学和蠕变性能。在三种蠕变载荷条件下，即225 ℃/30 MPa、225 ℃/35 MPa和275 ℃/35 MPa，在ARB过程中材料的界面处形成了厚度约17 μm的原子扩散层。生成的金属间化合物导致Al附近的界面厚度增加了40%。在恒温下，应力水平降低了13%，对界面厚度没有显著影响，蠕变失效时间缩短了44%。在恒定温度下，蠕变曲线的第二斜率随着应力水平的增加而达到39%，然后随着温度的小幅升高而降至2%。在275 ℃/35 MPa下进行蠕变试验，样品含60%Al和40%Cu，界面处有脆性的Al_2Cu金属间化合物。实验温度和应力对蠕变性能有影响，特别是应力越高，蠕变曲线的斜率越大。此外，通过晶体结构检测到动态再结晶。

关键词：蠕变性能；金属间化合物；累积辊压；微观结构；双金属片